JOURNAL OF GEOPHYSICAL RESEARCH, VOL. 104, NO. D18, PAGES 22,271-22,285, SEPTEMBER 27, 1999

Channel selection for soil spectrum reconstruction in 8-13 μm region

Zhao-Liang Li, F. Becker,[1] and M.P. Stoll

Laboratoire des Sciences de l'Image, de l'Informatique et de la Télédétection, Illkirch, France

Zhengming Wan and Yulin Zhang

Institute for Computational Earth System Science, University of California, Santa Barbara

Abstract. On the basis of the method developed by *Price* [1990] for selecting a limited number of channels to best represent the high-resolution spectra of materials within a spectral region, this paper presents a simplified procedure to reconstruct such spectra directly from their spectral measurements in the selected channels. Applying this procedure, it is shown that spectral reflectivities of more than 50 soil and vegetation samples measured in the laboratory at Johns Hopkins University (JHU) can be reconstructed using six selected channels in the 8-13 μm spectral region with an uncertainty of 0.005. It is also shown that the process of spectral channel selection proposed in this paper minimizes the propagation of measurement error to the whole reconstructed spectrum. Thus, if the reconstruction of spectrum is nearly insensitive to a small change in the center wavelengths and widths of the selected channels, the resulting errors on this reconstructed spectrum due to the measurement errors are increased by such a change. In order to validate this approach, the channels selected using the JHU data set are used to reconstruct the spectral data measured at the University of California at Santa Barbara for 43 types of soils. The results showed that the soil reflectance spectrum could be reconstructed by the channel reflectance measured in these six channels with their basis functions to within 0.005 almost over the full spectral range except for wavelengths around 8.6 μm and 9.5 μm for which the reconstruction is within 0.009. It should be kept in mind that these results refer to laboratory spectral data but not to remote sensing data where additional uncertainties will come from radiometric noise, errors associated with radiometric calibration, atmospheric corrections, and temperature/emissivity separation. Appreciable future work therefore has to be done with remote sensing data.

1. Introduction

Recent developments in detector technology and microelectronics make it possible to design high spectral resolution radiometers permitting the identification of narrower spectral features of target. However, such high spectral or hyperspectral resolution implies a cost both in money and in loss of other capabilities that might be offered through design trade-offs. Moreover, interband correlation may exist in high spectral resolution data which provide redundant data and reduce the signal to noise ratio. The questions that have to be addressed are what is the minimum number of spectral channels necessary for a particular application and how to choose the central wavelength position and spectral width of those channels. To answer these questions, *Price* [1975] developed an iterative procedure to analyze the spectra measured from space by infrared interferometer spectrometer (Iris) onboard Nimbus 4 satellite. He showed that it was adequate to determine the spectral variability in the spectral domain 6.25-25 μm with nine wide spectral bands. Using the same procedure but for the analysis of the reflectance spectra from more than 500 soil samples in the visible and near-infrared spectral domain, *Price* [1990] showed that it could be possible to reconstruct the spectra of soils with a few well selected channels in this domain. In recent years, a large number of measurements of spectral emissivity of natural media in the spectral range 8-13 μm have been performed in the laboratory [*Salisbury and D'Aria,* 1992; *Salisbury et al.,* 1994; *Snyder et al.,* 1997], and large spectral emissivity variations are observed in 8-13 μm; moreover, several thermal infrared spectral radiometers will be launched or are in progress, such as the advanced spaceborne thermal emission and reflectance radiometer (ASTER) [*Kahle et al.,* 1991]. The determination of optimal bands to analyze particular features is becoming very timely.

The questions as to whether the selection of channels obtained from Price's method is unique and optimal are therefore crucial. In other words, using Price's procedure, is it possible to select several sets of channels that would lead to the same reconstruction of the spectra with the same uncertainty? The answers to these questions are complex and depend not only on the spectral characteristics of the materials but also on the atmosphere and the temperature/emissivity

[1] Also at International Space University, Illkirch, France.

Paper number 1999JD900479.
0148-0227/99/1999JD900479$09.00

separation methods as well as on the noise of the radiometer. These important questions deserve a careful study that is in progress and will therefore not be addressed in detail in this paper, which will be concerned with a first approach to their solution. Since the answer to these questions depends on the noise of the instrument, it is necessary to have a method which is based on the quantities actually measured. We propose therefore in the second section of this paper an extension of Price's approach to determine the minimum spectral channels necessary to reconstruct a complete spectrum from laboratory reflectance (emissivity) measured in these spectral channels. Although the method proposed is general, we apply it, in section 3, to the selection of spectral channels for soil and vegetation spectra reconstruction in the spectral region 8-13 μm using laboratory data. Two independent laboratory spectral data sets are used as a practical example to select the minimum channels and to validate the method. This is only an example; there are other types of spectral analysis which can be performed such as mineral and rock analysis. There are other spectral regions to be considered such as 3-5 μm [*Salisbury and D'Aria,* 1994]. As a consequence, the practical results obtained in section 3 will not be applicable without extension to these situations. Furthermore, since this paper uses laboratory data as an illustration, the practical results obtained cannot be extended to remote sensing data without addressing, for instance, the problems related to atmospheric corrections and temperature/emissivity separation. Therefore the selection of channels proposed in the example in this paper may not be optimal for those more general situations, and the procedure proposed has to be extended to those cases, which implies that appreciable future work be done in this respect. For instance, in order to give some order of the magnitude of the impact of the atmospheric effects on the choice of channels, we discuss in section 3 the impact of the displacement of channels which are in the ozone and water vapor absorption bands. Section 4 is then devoted to a sensitivity study and an error analysis. To this end, we introduce statistical noise in the data measured in the selected channels, and we analyze the impact of the choice of the selected channels on the error generated in the reconstructed spectrum. This leads to a criterion of optimization which is briefly discussed. Finally, some potential applications are discussed in section 5.

2. Channel Selection Procedure and Spectral Reconstruction

Considering that all spectral bands are not independent, it may be possible to identify a set of independent (uncorrelated) channels from which all other can be derived. A method for such an identification has been developed by *Price* [1975] and applied to spectra from satellite instrument Iris and to laboratory and field reflectance spectra in visible and near-infrared by the same author [Price, 1990, 1994, 1997].

2.1. Price's Procedure

Let $x^\alpha(\lambda) = (x_1^\alpha, x_2^\alpha, ..., x_n^\alpha)$ represent the spectral signature of material α measured over the set of n wavelength values $\lambda = (\lambda_1, \lambda_2, ..., \lambda_n)$, where n is assumed to be high enough to resolve all spectral features. The principle of Price's method is to express the spectrum $x^\alpha(\lambda)$ as the weighed sum of M spectral basis function $\varphi_i(\lambda)$ in appropriately selected channel i, namely,

$$x^\alpha(\lambda) \cong \sum_{i=1}^{M} S_i^\alpha \varphi_i(\lambda), \tag{1}$$

where the weights S_i^α are wavelength integrals related to the original spectrum $x^\alpha(\lambda)$ and the basis functions $\varphi_i(\lambda)$ are spectral shapes (independent on the material α) defined from statistical analysis of a collection of spectra and M is the number of basis functions (channels) required to describe the $x^\alpha(\lambda)$ to within very small residuals. The procedure developed by Price is an iterative approach. The first iteration assumes that expression (1) reduces to one channel only and both S_1^α and $\varphi_1(\lambda)$ are determined. At (i-1)th iteration, it is assumed that

$$x^\alpha(\lambda) \cong \sum_{j=1}^{i-1} S_j^\alpha \varphi_j(\lambda),$$

and we calculate at ith iteration the residuals

$$\delta x_i^\alpha(\lambda) = x^\alpha(\lambda) - \sum_{j=1}^{i-1} S_j^\alpha \varphi_j(\lambda)$$

by introducing new channel weight S_i^α and new channel basis function $\varphi_i(\lambda)$ such that

$$\delta x_i^\alpha(\lambda) = S_i^\alpha \varphi_i(\lambda).$$

At each iteration, the approach consists of two phases.

2.1.1. Phase 1: Selection of channel position. Since the number of wavelengths representing the high-resolution spectrum may be vary large, the inversion of the very high dimensionality matrices involved in the process is computationally intensive and subject to runoff errors. Furthermore, existence of noise and spectral redundancy in the data lead to failure in matrix inversion, and the standard methods for spectral analysis, such as principal components analysis, encounter difficulties. In order to overcome these difficulties, the first step in this phase is to use the Gram-Schmidt procedure to select a limited set (L, $L<<n$) of preliminary basis vectors which provide an acceptable approximation to the actual set of the spectral data.

Let $\delta x_i^\alpha(\lambda)$ be the residual vector at (i-1)th iteration, which is the difference between the measured spectrum of material α and the approximate expansion of this spectrum to order i-1 such as

$$\delta x_i^\alpha(\lambda) = x^\alpha(\lambda) - \sum_{j=1}^{i-1} S_j^\alpha \varphi_j(\lambda). \tag{2}$$

We use the Gram-Schmidt procedure to construct a set of L Gram-Schmidt unit vectors $e_h(\lambda)$ (h=1,L) from the residuals vectors $\delta x_i^\alpha(\lambda)$ so that for all spectra the residuals vectors may be represented by these L Gram-Schmidt vectors:

$$\delta x_i^\alpha(\lambda) = \sum_{h=1}^{L} c_h^\alpha e_h(\lambda) + r^\alpha(\lambda),$$

where $r^\alpha(\lambda)$ is the residuals and c_h^α is the inner product of the two vectors $e_h(\lambda)$ and $\delta x_i^\alpha(\lambda)$ defined by

$$c_h^\alpha = \sum_{k=1}^{n} e_h(\lambda_k)\, \delta x_i^\alpha(\lambda_k),$$

and, by construction, the vectors $e_h(\lambda)$ are a set of orthonormalized vectors according to the previous inner product.

From the coefficients c_h^α of these L basis vectors, the covariance matrix **C** whose component, C_{kh}, is constructed by

$$C_{kh} = \sum_{\alpha=1}^{N} c_k^\alpha c_h^\alpha \quad (k, h=1,L),$$

where N is the total number of samples. Then the principal-component analysis is applied to this LxL covariance matrix. From the component γ_{kh} of L eigenvectors of dimensionality L, plus the original basis vectors $e_h(\lambda)$ of dimensionality n, we construct approximate L eigenvectors $E_k(\lambda)$ of dimensionality n for the full spectra, that is,

$$E_k(\lambda) = \sum_{h=1}^{L} \gamma_{kh} e_h(\lambda).$$

Since the first eigenvector $E_k(\lambda)$ describes most of the data set's variability, a spectral region where the absolute value of the first eigenvector is large takes into account most of this variability, and the channel central wavelength must be chosen in this spectral region. The choice of the channel central wavelength and width in this spectral region (interval) is the result of a trade-off between the width of channel and the signal-to-noise ratio. In fact, if a narrow channel increases the ability to identify a narrow spectral feature, it reduces the signal-to-noise ratio compared with a broader channel. Such a trade-off for the remote sensing instrument should consider the atmospheric properties. Considering realistic values of channel widths in the thermal infrared domain (such as those of the most recent thermal infrared radiometers), we choose in the practical example channel widths varying from 0.3 μm to 0.5 μm depending on the sharpness around the maximum value of the first eigenvector. Figure 2 illustrates, for our case study, the spectral variation of the largest eigenvector (largest eigenvalue) at each step of the iteration and the positions of the selected channels indicated by the bars labeled in channel numbers (the height of the bars have no meaning). One notes in Figure 2 that some maxima are sharp, while others are smoother.

2.1.2. Phase 2: Determination of the spectral basis function $\varphi_i(\lambda)$. Knowing the interval of channel i, $\lambda_{i\min}, \lambda_{i\max}$ (the lowest and highest wavelength values for channel i, respectively), the coefficients S_i^α are computed as the mean value of $\delta x_i^\alpha(\lambda)$ over this interval:

$$S_i^\alpha = \frac{1}{\lambda_{i\max} - \lambda_{i\min}} \int_{\lambda_{i\min}}^{\lambda_{i\max}} \delta x_i^\alpha(\lambda)\, d\lambda = \int \delta x_i^\alpha(\lambda)\, d\lambda_i . \quad (3)$$

According to the principle of the method, the residual vector $\delta x_i^\alpha(\lambda)$ is approximated at ith iteration by

$$\delta x_i^\alpha(\lambda) = S_i^\alpha \varphi_i(\lambda); \quad (4)$$

therefore the basis functions $\varphi_i(\lambda)$ can be determined by the minimization of (4)

$$\varphi_i(\lambda) = \frac{\sum_{\alpha=1}^{N} \left[\delta x_i^\alpha(\lambda) S_i^\alpha\right]}{\sum_{\alpha=1}^{N} \left(S_i^\alpha\right)^2} \quad (5)$$

and can satisfy $\int \varphi_i(\lambda)\, d\lambda_i = 1$.

At this point, the procedure advances to the next iteration (i+1). The iteration of the process ends when the residual vectors have no observable pattern, or seem to be dominated by noise, or when a single eigenvector from the principal components analysis no longer explains a major part of the spectral variability. The steps of the process to calculate the eigenvectors, to select the channel positions and widths, to determine the basis functions $\varphi_i(\lambda)$, and to calculate the quantities S_i^α are detailed by *Price* [1990, 1994].

2.2. Extension of Price's Spectral Reconstruction Method

The method proposed by Price is powerful, but the calculations of the coefficients S_i^α from (3) are somewhat complicated, and furthermore the coefficients S_i^α are not simply related to the measured quantities as explained below. We propose in the following a simpler way to calculate these quantities which makes better use of this method and furthermore which allows us to express the emissivity or reflectivity directly in terms of the measured quantities. Once all channel positions and widths are defined by Price's procedure as described in section 2.1.1 (phase 1), an alternative method can be used to reconstruct directly the spectrum $x^\alpha(\lambda)$ with the quantities m_i^α measured in the selected channels. We express $x^\alpha(\lambda)$ directly in terms of m_i^α as follows:

$$x^\alpha(\lambda) = a_0(\lambda) + \sum_{i=1}^{M} m_i^\alpha a_i(\lambda), \quad (6)$$

where, by definition, m_i^α is the channel average of the spectral quantity $x^\alpha(\lambda)$ weighed by the spectral response function, $f_i(\lambda)$, of the detector in channel i, and is given by

$$m_i^\alpha = \frac{1}{\int_{\lambda_{i\min}}^{\lambda_{i\max}} f_i(\lambda)\, d\lambda} \int_{\lambda_{i\min}}^{\lambda_{i\max}} f_i(\lambda) x^\alpha(\lambda)\, d\lambda = \int f_i(\lambda) x^\alpha(\lambda)\, d\lambda , \quad (7)$$

$a_i(\lambda)$ is the spectral basis function predetermined from multiple regression of (6) over the whole data set, and M is the total number of channels used to approximate $x^\alpha(\lambda)$ by (1).

The advantage of (6) is that it uses directly the measured quantities m_i^α instead of S_i^α to reconstruct a spectrum. This avoids using the iterative procedure to compute S_i^α by Price's method.

In fact, assuming that $f_i(\lambda) = 1$ for comparison, we define

$$b_{ij} = \int \varphi_j(\lambda)\, d\lambda_i \qquad b_{ii} = 1$$

so that b_{ij} is the integral over the ith spectral domain of the jth basis function. By inserting (2) into (3), it is easy to show that the S_i^α can be written as

$$S_i^\alpha = \sum_{j=1}^{i} d_{ij} m_j^\alpha$$

with

$$d_{ii} = 1 \qquad d_{ij} = -\sum_{k=j}^{i-1} b_{ik} d_{kj} \qquad j < i$$

which transforms (1) into

$$x^\alpha(\lambda) = \sum_{i=1}^{M} m_i^\alpha a_i(\lambda) \quad (8)$$

with

$$a_i(\lambda) = \sum_{j=i}^{M} d_{ji} \varphi_j(\lambda) \quad (9)$$

$$\int a_i(\lambda)\, d\lambda_i = 1 .$$

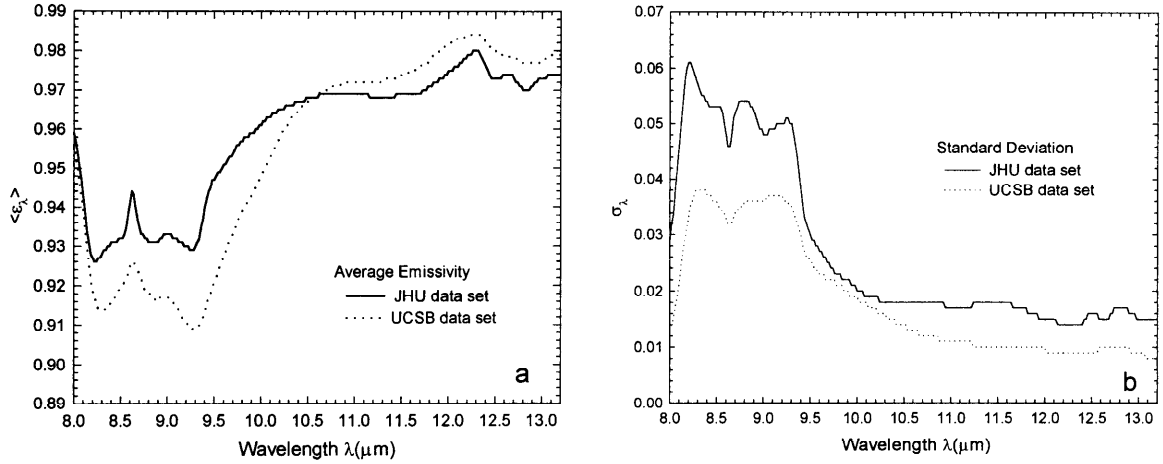

Figure 1. General properties of the emissivity spectra for Johns Hopkins University (JHU) and University of California at Santa Barbara (UCSB) data sets of soil, vegetation, water, and snow samples: (a) mean emissivity spectrum and (b) standard deviation of emissivity for each wavelength.

Note that the only difference between (8) and (6) is that the latter one has one more function $a_0(\lambda)$. This function is, indeed, very small in terms of reflectivity (<0.004) over the whole spectral range as shown in Figures 8 and 9.

Another difference with Price's approach is that in Price's approach the channel basis functions $\varphi_i(\lambda)$ are determined iteration by iteration. It means that the choice of channel $i+k$ has no impact on the function $\varphi_i(\lambda)$. In our approach, since the minimization leading to the spectral basis function $a_i(\lambda)$ is global, there is an impact of the choice of channel $i+k$ on $a_i(\lambda)$. This makes the method more stable and gives some control over error propagation as will be discussed in section 4.

From the definition of m_i^a (expression (7)), the functions $a_i(\lambda)$ have the follow properties:

$$\int a_k(\lambda) f_i(\lambda)\, d\lambda_i = \delta_{ik}$$

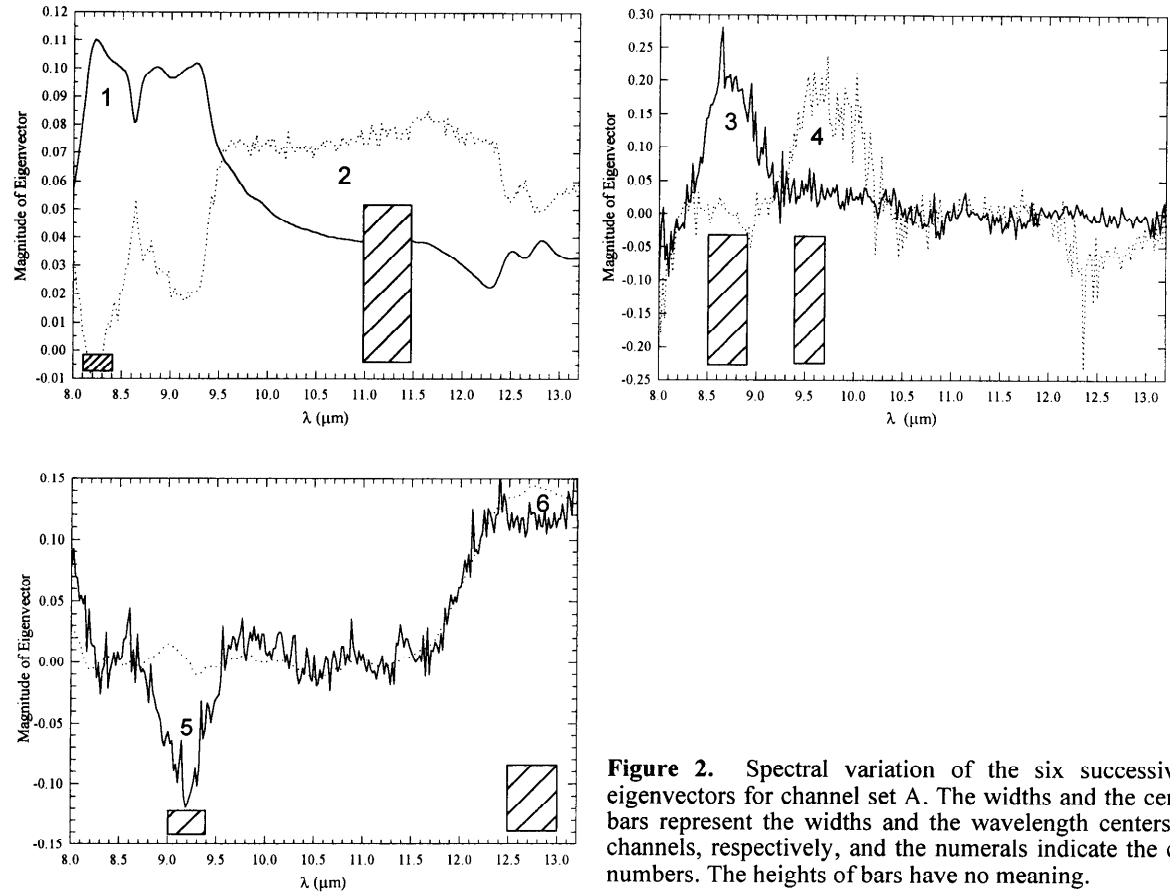

Figure 2. Spectral variation of the six successive first eigenvectors for channel set A. The widths and the centers of bars represent the widths and the wavelength centers of the channels, respectively, and the numerals indicate the channel numbers. The heights of bars have no meaning.

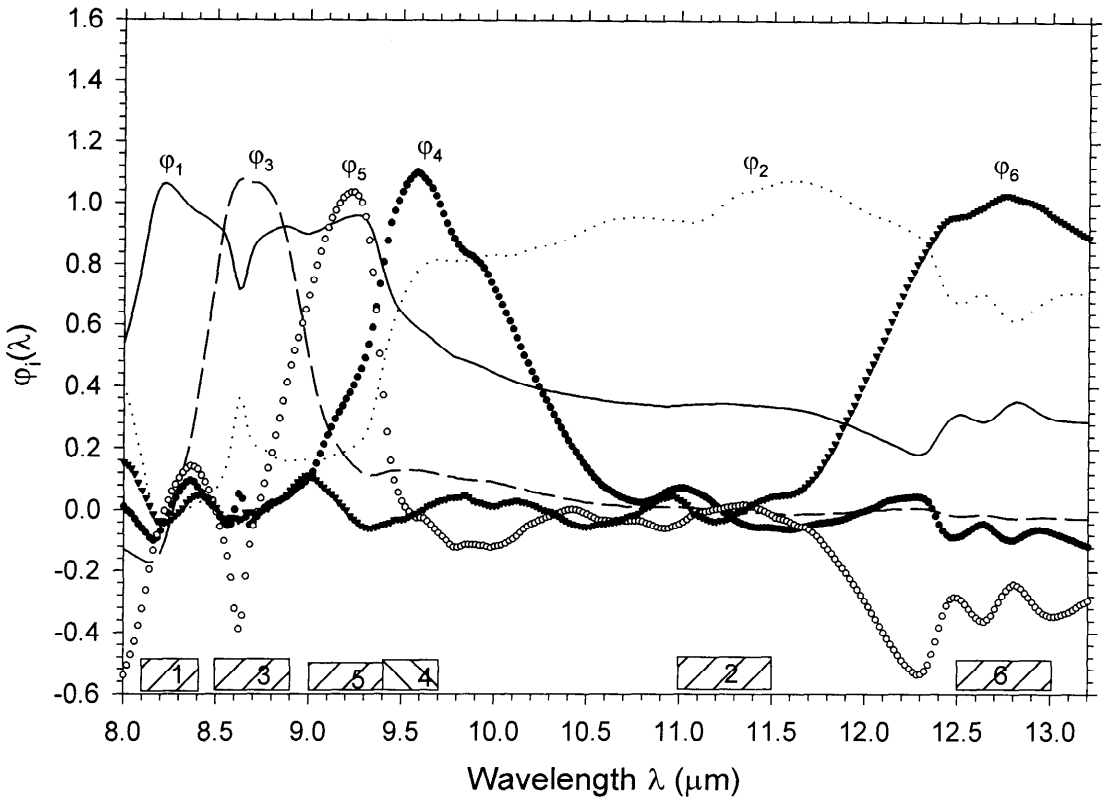

Figure 3. Spectral basis functions $\varphi_i(\lambda)$ with associated channel positions and widths (bars) for channel set A. Numerals in each bar indicate the channel number.

where δ_{ik} is the Kronecker symbol ($\delta_{ii}=1$ and $\delta_{ik}=0$ if $k \neq i$). In other words, the average of the function $a_k(\lambda)$ in each of the spectral domains $k \neq i$ is null. For our analysis, $x^{\alpha}(\lambda)$ will be either the spectral emissivity $\varepsilon(\lambda)$ or the spectral hemispheric reflectivity $\rho(\lambda)$ in the case of spectral signature reconstruction. Since $\varepsilon(\lambda)=1-\rho(\lambda)$ according to Kirchhoff's law for opaque media, only $\rho(\lambda)$ will be used in this paper.

3. Application to Laboratory Spectral Data Sets

The application of the method focuses on soil, vegetation, water, and snow, which are essential components of the terrestrial ecosystem. Minerals and rocks will be considered in the future.

Two data sets were used in this study. One consists of 53 spectra measured in the laboratory at Johns Hopkins University (JHU) for different soil, vegetation, and snow samples. Sampling locations and brief physical descriptions of these samples were given by *Salisbury and D'Aria* [1992]. Suffice it to say here that these soil samples were obtained from all over the United States except for the aridisols which come primarily from the Middle East. Another data set contains 43 spectra measured in the laboratory at the University of California at Santa Barbara (UCSB) for different soil samples obtained mainly from different places in California, Nevada, and Maryland. All spectra in these two data sets are the spectral variation of directional hemispherical reflectance measured in the laboratory by the use of an integrating sphere and a thermal infrared spectrometer. The methodology of the collection of soils samples and their measurements as hemispherical reflectance are well documented by *Salisbury and D'Aria* [1992] and *Snyder et al.* [1997]. In this study, the JHU data set is used to select the minimum number of channels (positions and widths) necessary to best reconstruct soil spectra in 8-13 μm and to determine their associated basis functions, whereas the UCSB data set is used for evaluating the performance of the proposed method.

3.1. Spectral Emissivity Variation of Soil and Agricultural Surfaces in the 8~13 μm Region

The general properties of the spectra for these two data sets are displayed in Figure 1. Figure 1a shows the spectral variation of the average emissivity computed from the JHU and the UCSB data sets, and Figure 1b displays the corresponding spectral variation of the second moment of these data sets.

It is interesting to note the following for a given data set: (1) For given wavelength, the larger the variation of emissivity is, the smaller the average emissivity is. (2) The longer the wavelength is, the smaller the variation of emissivity is. (3) The variation of emissivity for a wavelength greater than 10 μm is about 0.02; this may lead to an error of 1.2 K on surface temperature [Becker, 1987]. (4) There are no simple analytical expressions to model these spectral variations. The spectral shapes of the average emissivity and the second moment of spectral emissivity in the two data sets

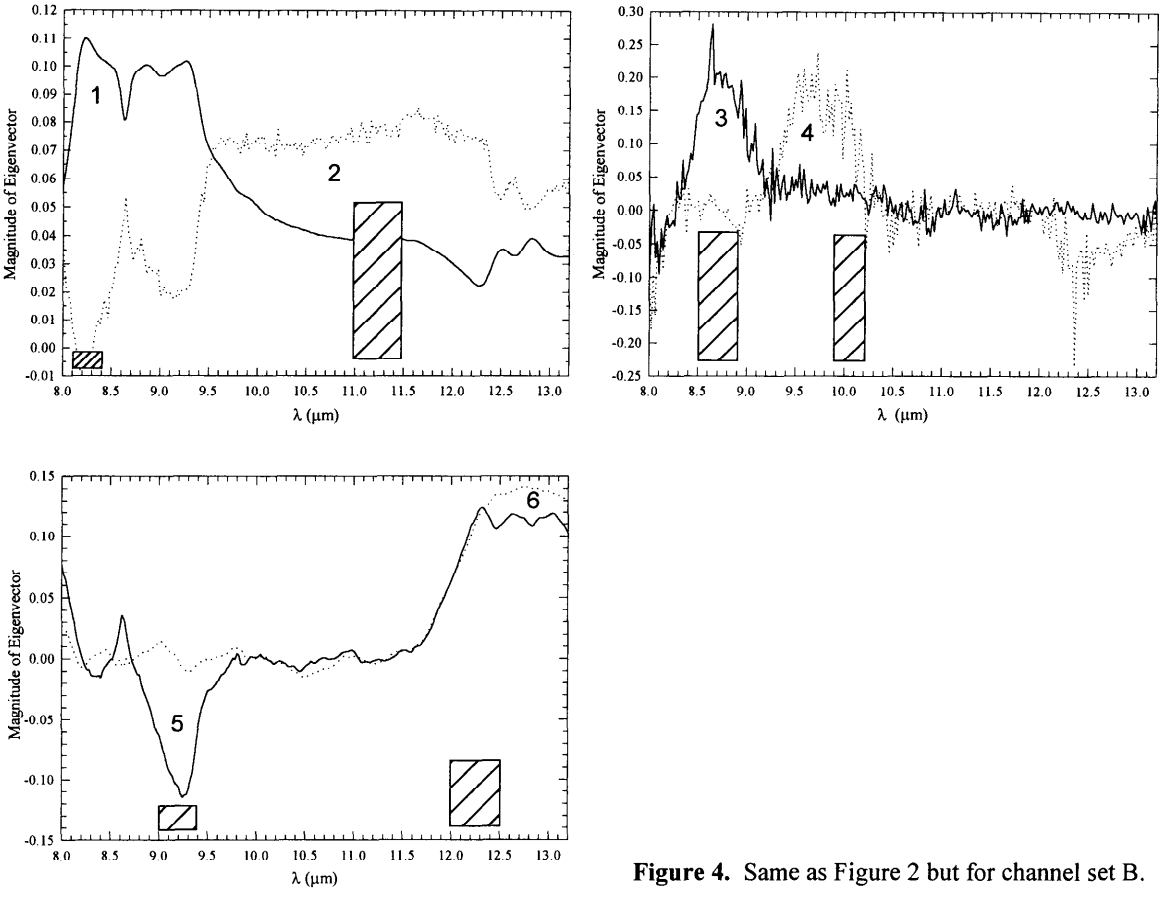

Figure 4. Same as Figure 2 but for channel set B.

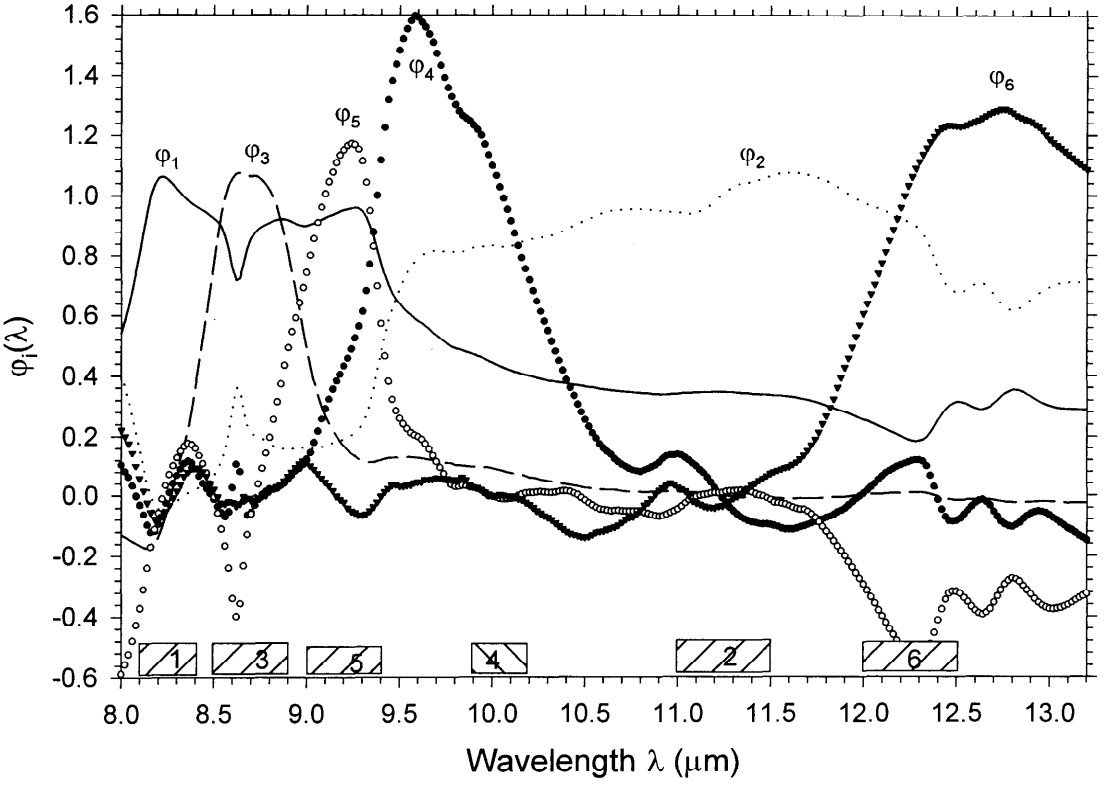

Figure 5. Same as Figure 3 but for channel set B

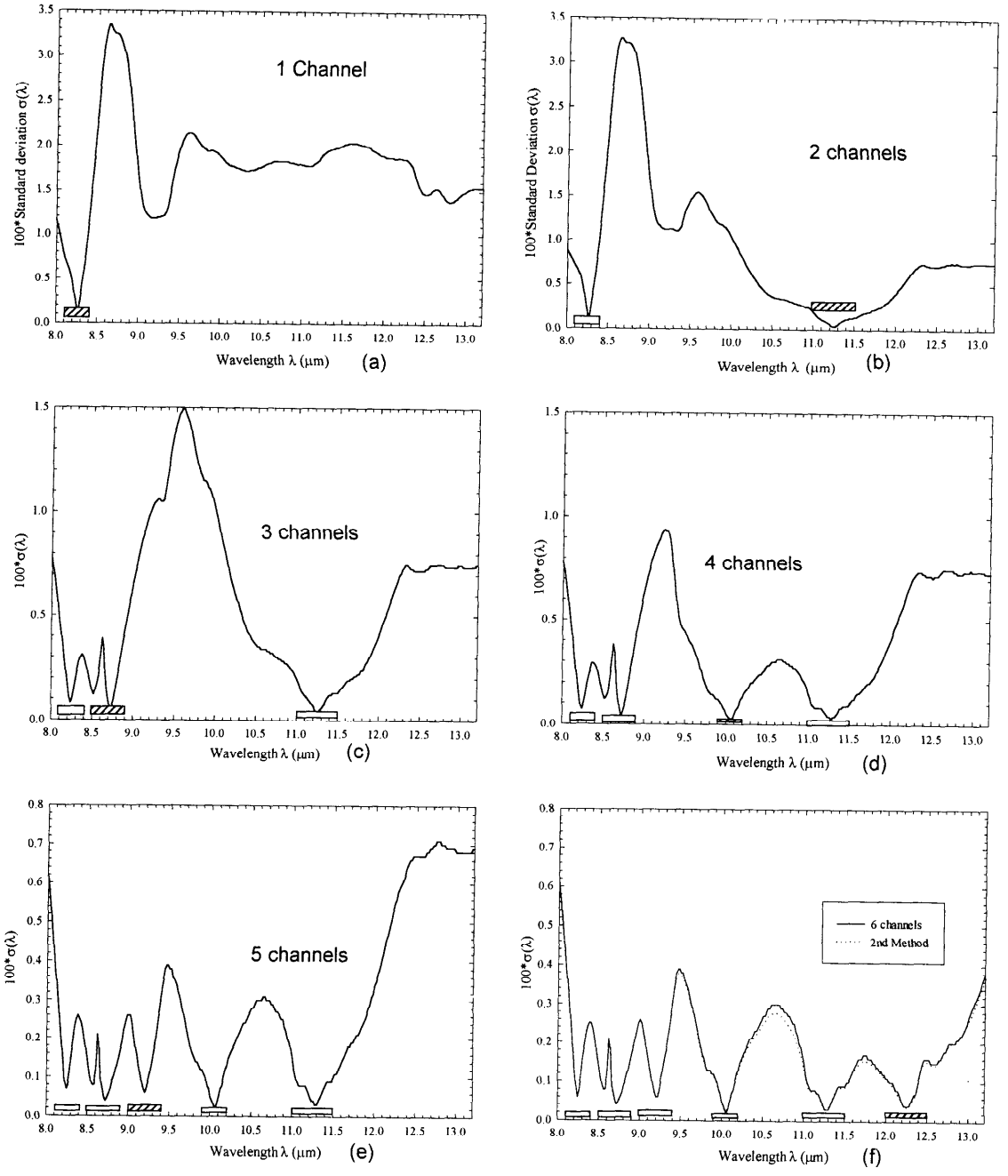

Figure 6. Standard deviation for each wavelength between the measured and reconstructed reflectance spectra using set B of selected channels: (a) one channel, 8.1-8.4 μm; (b) two channels, 8.1-8.4 μm and 11.0-11.5 μm; (c) three channels, 8.1-8.4 μm, 11.0-11.5 μm, and 8.5-8.9 μm; (d) four channels, 8.1-8.4 μm, 11.0-11.5 μm, 8.5-8.9 μm, and 9.9-10.2 μm; (e) five channels, 8.1-8.4 μm, 11.0-11.5 μm, 8.5-8.9 μm, 9.9-10.2 μm, and 9.0-9.4 μm; (f) six channels, 8.1-8.4 μm, 11.0-11.5 μm, 8.5-8.9 μm, 9.9-10.2 μm, 9.0-9.4 μm, and 12.0-12.5 μm. The dotted curve represents the standard deviation obtained using equation (6) with the six channels. The bars represent the channel positions and widths as indicated in Figure 5.

are similar, even though they are obtained from measurements of different samples with different instruments.

3.2. Selection of Channels

In order to test our method, Price's procedure described above was first applied to the reflectance spectra measured in the laboratory by *Salisbury et al.* [1992] (JHU data set). The iteration has been stopped after the selection of the sixth channel, because at the seventh iteration there is no dominant eigenvector which can explain the major part of the spectral variability. Figure 2 illustrates the successive first eigenvectors together with the associated channel positions and widths, while the spectral basis function $\varphi_i(\lambda)$ and associated channels are shown in Figure 3. This set of selected channels will be referred to as channel set A in the following. Figure 2 shows that one of the channels of set A (channel 4) is

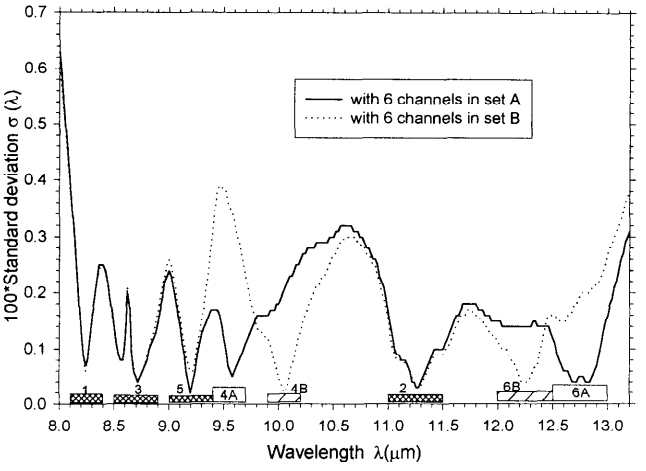

Figure 7. Standard deviation for each wavelength between the measured and reconstructed reflectance spectra using sets A and B of selected channels. The bars represent the channel positions and widths. Numerals indicate the channel numbers.

right in the ozone absorption band, while another one (channel 6) is in the water vapor absorption band.

Although we do not include the atmospheric effects in our studies, we want to study the impact of the displacement of the selected channels which may be necessary for remote sensing. The spectral regions corresponding to the strong ozone absorption in the atmosphere at 9.4 to 9.8 μm and the strong water vapor absorption above 12.5 μm have been excluded in a second channel selection procedure. For this reason, the positions of channels 4 and 6 have been shifted out of the absorption band, but they are as close as possible to the regions where the corresponding eigenvectors have the larger values. The successive first eigenvectors and the spectral basis function $\varphi_i(\lambda)$ for this new channel set, referred to as channel set B in the following, are displayed in Figures 4 and 5, respectively.

In order to illustrate how the method works, Figure 6 displays the residual standard deviation error on signatures resulting from increasing the number of channels used for reconstructing the spectrum with the channel set B. Figure 6a shows the residual standard deviation error using only one channel. Figures 6b-6f show how successive introduction of a new channel reduces the residual error. It can be observed that with the four first channels of the channel set B, the largest standard deviation does not exceed 0.01, and with six channels of the channel set B, it does not exceed 0.005. The addition of a seventh channel would have not improved this result, although it may lead to a better reconstruction locally around this channel position. Figure 7 compares the residual standard deviation errors obtained using six channels of the channel set A with that obtained using the channel set B. It turns out that both set A and set B yield very similar results and lead to equivalent uncertainties when there are no errors introduced in the measurements (we shall see in section 4 that when such errors are introduced, set A generates smaller errors). The differences occur mainly in the spectral region selected for channels 4 and 6, and the minima correspond obviously to the channels selected for the measurements.

We then applied to the same data set the method which we proposed in this paper (equation (6)). The results are shown on Figure 6f by the dotted curve noted "second method" results. One can see from Figure 6f and Table 1 that our approach gives the same reconstructed values as those produced by Price's approach, although the $a_i(\lambda)$ shown on Figure 8 for channel set A and on Figure 9 for channel set B are different from the $\varphi_i(\lambda)$ (Figures 3 and 5) as demonstrated by (9). Comparing Figure 8 with Figure 9, one notes that the positions of the maxima of the basis functions $a_i(\lambda)$ for channels 4 and 6 are independent of the positions of the selected channels and are always at the spectral regions where their corresponding first eigenvectors are large. Furthermore, the maxima of the basis functions $a_i(\lambda)$ for channels 4 and 6 in channel set B are larger than that in channel set A. This results from the fact that $\int a_i(\lambda)\,d\lambda_i$ must be equal to unity, although the channel i does not correspond

Table 1. Unexplained Variance and Cumulative Percentage Variance Described by M Channels With Two Different Methods

Iteration/Channel M	Unexplained Variance: Var(M)*		Cumulative Variance Described, CVar(M),+ %	
	Price (Equation (1))	This study (Equation (6))	Price (Equation (1))	This study (Equation (6))
0	1583.4	1583.4	0	0
1	181.6	122.0	88.5	92.3
2	72.9	67.4	95.4	95.7
3	24.3	22.8	98.5	98.6
4	11.4	11.3	99.3	99.3
5	6.8	6.5	99.6	99.6
6	2.2	2.1	99.9	99.9

* Var(M) represents the unexplained variance (M) defined as $\sum_{\alpha=1}^{N}\int_{8.0}^{13.2}\left(\delta x_M^{\alpha}(\lambda)\right)^2 d\lambda$, where M is the total number of channels, N is the total number of samples, $\delta x_M^{\alpha}(\lambda)=x^{\alpha}(\lambda)-\sum_{i=1}^{M}S_i^{\alpha}\varphi_i(\lambda)$ for Price's method (see (1)), and $\delta x_M^{\alpha}(\lambda)=x^{\alpha}(\lambda)-a_0(\lambda)-\sum_{i=1}^{M}m_i^{\alpha}a_i(\lambda)$ for our method (see (6)).

+ CVar(M) is the cumulative percentage variance described by M channels defined as $100.0-\frac{\text{Var(M)}}{\sum_{\alpha=1}^{N}\int_{8.0}^{13.2}\left(x^{\alpha}(\lambda)\right)^2 d\lambda}100.0$.

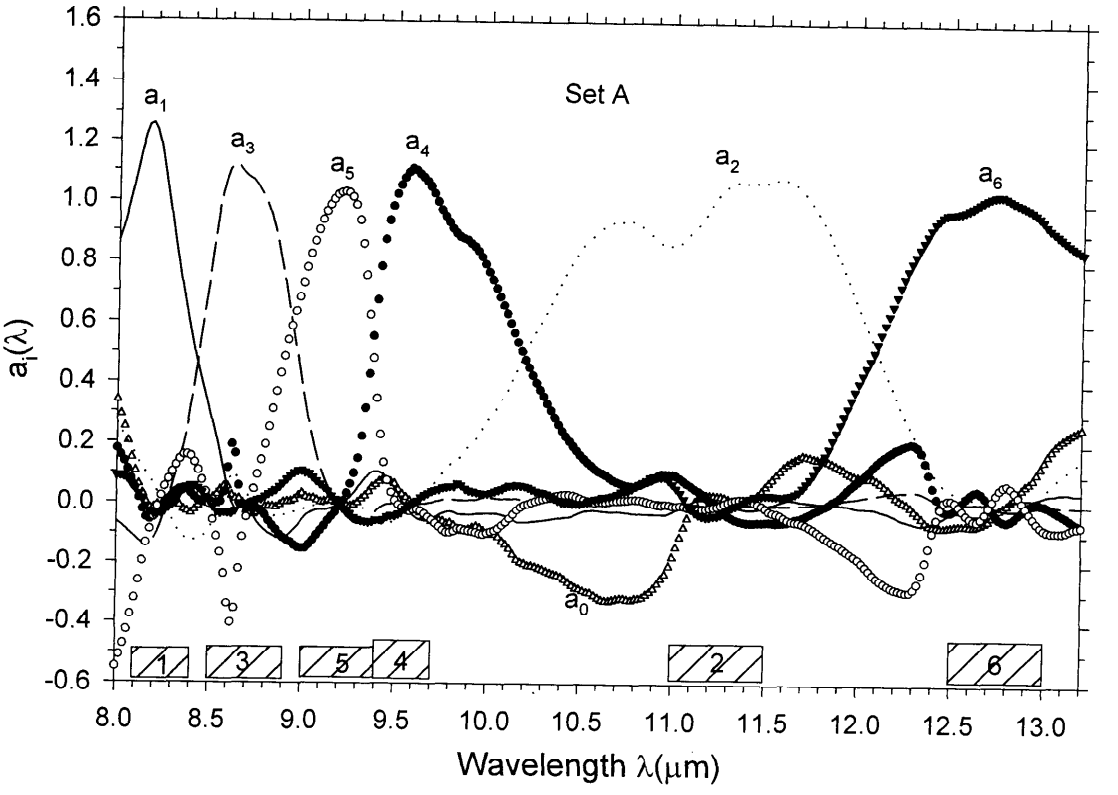

Figure 8. Spectral variation of six spectral basis functions $a_i(\lambda)$ determined by minimization of equation (6) for channel set A over the whole JHU data set. The bars represent the channel positions, and the numerals indicate the channel number.

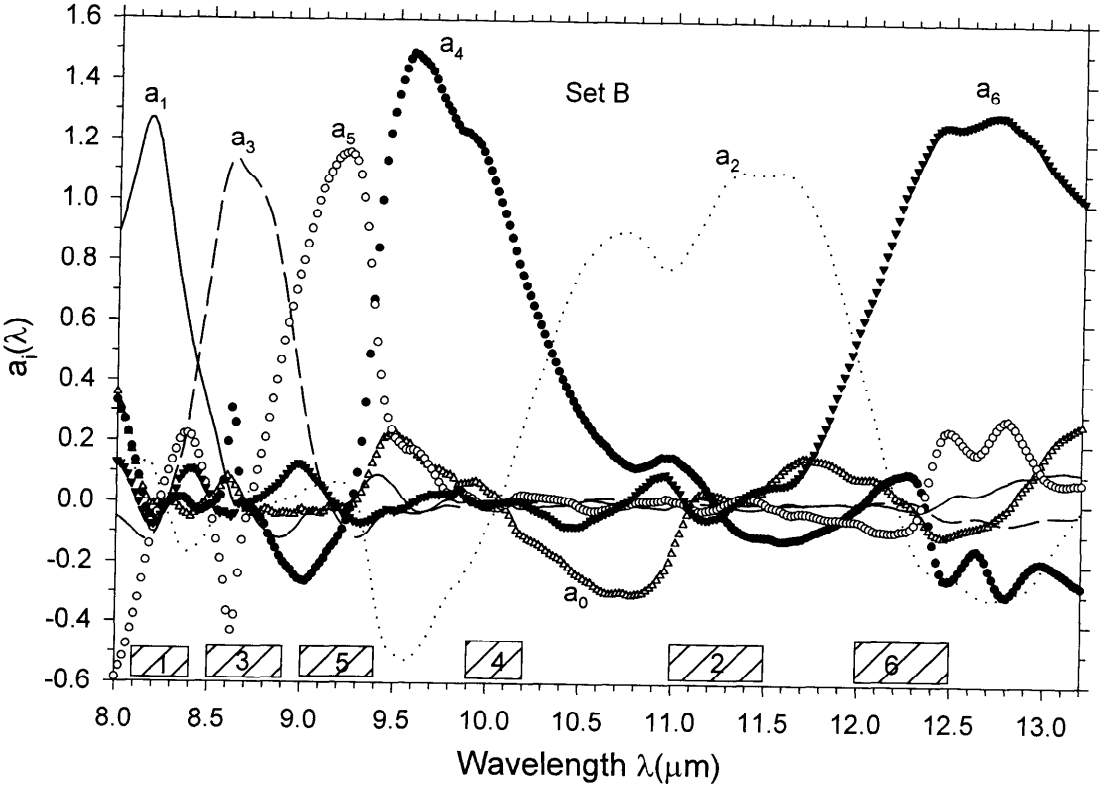

Figure 9. Same as Figure 9 but for channel set B.

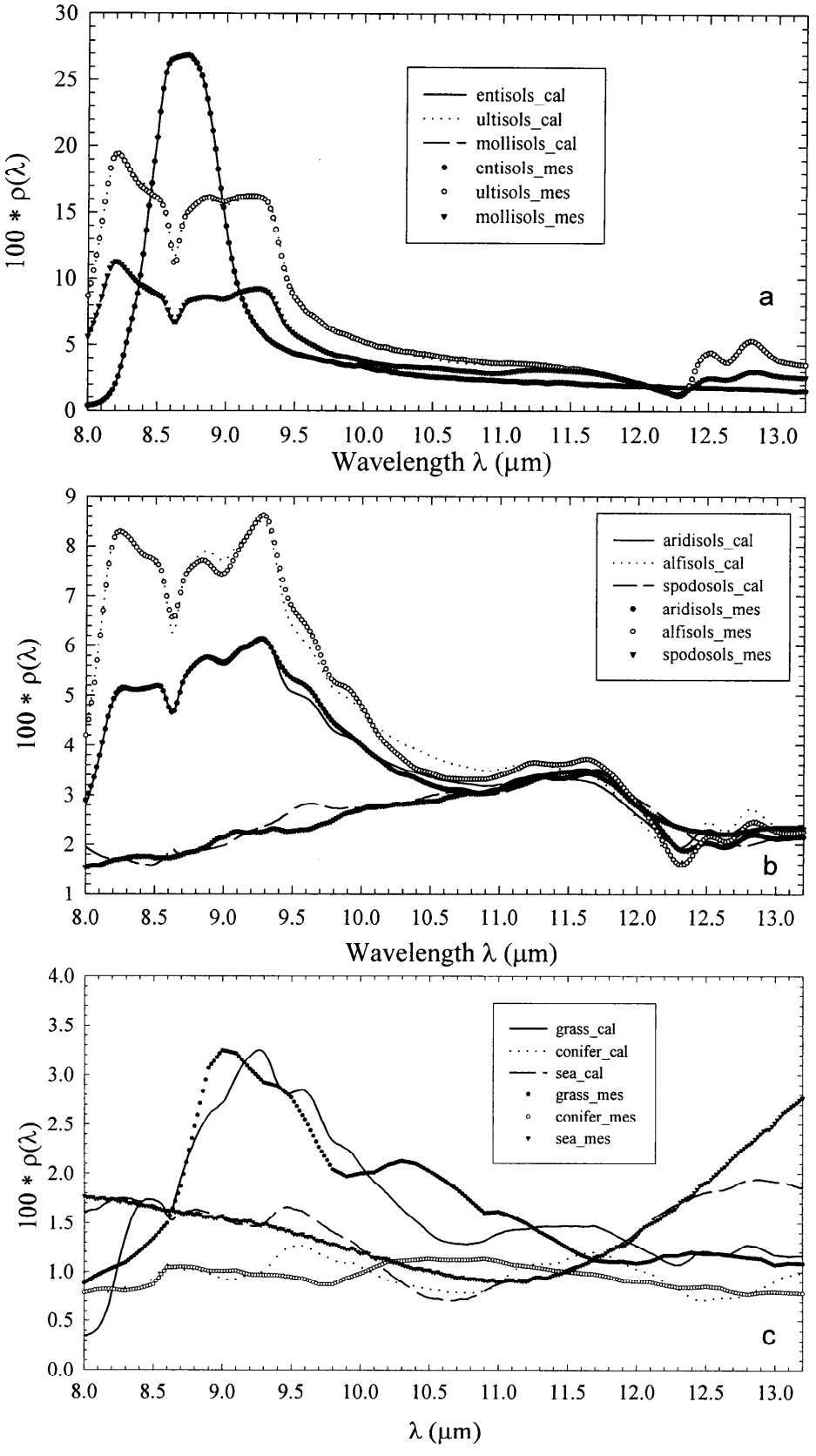

Figure 10. Measured (symbols) and reconstructed (lines) reflectance spectra for (a) and (b) a few soil samples and (c) a few vegetation and water samples.

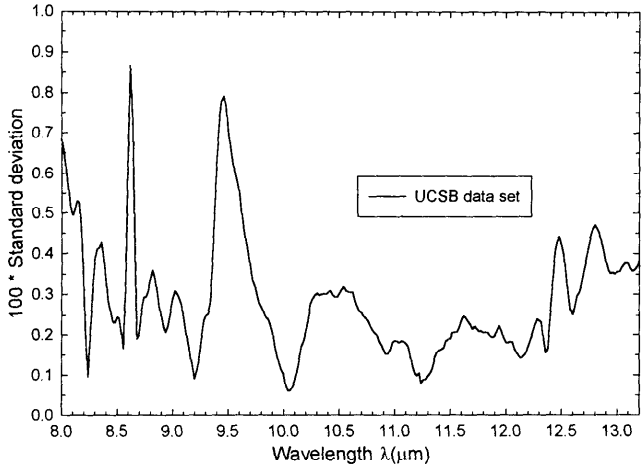

Figure 11. Standard deviation for each wavelength between the reconstructed and measured spectra for the 43 soil samples in the UCSB data set. Note that the spectra are reconstructed by equation (6) using $a_i(\lambda)$ determined with the JHU data set.

to the maximum of $a_i(\lambda)$. This has an important impact on the error propagation discussed in section 4. We see also that if the function $a_i(\lambda)$ is not null within channel k, $a_i(\lambda)$ values change their signs within this channel in order to insure $\int a_i(\lambda)\, d\lambda_k = 0$. It is also interesting to note that forcing channel 4 to be outside of the theoretically selected spectral domain has no impact on the positions of channels 5 and 6 as it is seen by comparison of Figures 2 and 4.

3.3. Results of Spectrum Reconstruction

3.3.1. JHU data set. We have tested the efficiency of our approach on the JHU data set for control using the channel set B of selected channels (which takes into account the ozone and water vapor absorption bands). Figure 10 presents a few examples of reconstructed signatures (in the 8-13 μm band) based on the six selected channels (channel set B) and their corresponding spectral basis functions. The reconstruction is excellent in all cases; it is extremely good for all soil spectra. The reason is that the soil signatures are correlated because most of the spectral features occur in the same regions, being associated with the relative abundance of silicates and carbonates plus a few minor constituents. Contrarily, the "worst" results are observed with vegetation signatures that are not correlated to mineral spectral features. Probably, the vegetation signatures are not correlated among themselves.

3.3.2. UCSB data set. The reconstruction technique (equation 6) was applied to the UCSB data set to evaluate the performance of the developed procedure because the UCSB data set is independent of the JHU data set. First, using (7), we simulated the measured quantities m_i^{α} in each of the six selected channels of set B for each sample α in the UCSB data set, then we reconstructed all spectra using (6) with the coefficients (basis functions) $a_i(\lambda)$ determined with the JHU data set and given in Figure 9. Figure 11 displays the standard deviation for each wavelength between the reconstructed and measured reflectance spectra. It can be seen that (6) reconstructs spectra to within 0.005 for almost the full spectral range except for wavelengths around 8.6 μm and 9.5 μm for which the reconstruction is within 0.009. As was done in Figure 10 for the JHU data set, a few examples of reconstructed signatures in the 8-13 μm region for the UCSB data set are displayed in Figure 12. The reconstruction is not as good as that for the JHU data set. The reasons for this are as follows: (1) The fifty soil samples in the JHU data set used to determine the channel positions, widths, and the associated spectral basis functions were obtained mainly over the United States; they represent certainly a fraction of the types of soils present in the world. It could be possible that some types of soils in the UCSB data set are not found in the JHU data set. (2) The use of the small data samples (50 samples) produces less than optimal results; therefore larger samples would have yielded more efficient results. In order to improve the reconstruction, such an analysis of the differences between reconstructed and measured reflectance spectra may be used to select more channels using the proposed method.

4. Sensitivity Study and Error Analysis

4.1. Sensitivity Analysis

In order to show how the spectrum reconstruction is sensitive to the chosen center wavelengths and widths of the selected channels, the spectral residual standard deviations were calculated using three sets of selected channels modified with respect to channel set A as follows: In set 1, the channel widths w are unchanged, but the center wavelengths λ_c of all channels are shifted toward the lower value by 0.1 μm. ($\Delta w = 0$ and $\Delta\lambda_c = -0.1$ μm). In set 2, the center wavelengths are unchanged, but the channel widths of all channels increased by 0.2 μm ($\Delta w = 0.2$ μm and $\Delta\lambda_c = 0$). In set 3, both the channel widths and center wavelengths of all channels changed ($\Delta w = 0.1$ μm, $\Delta\lambda_c = -0.05$ μm).

Figure 13 displays the spectral residual standard deviation for these three cases and that for the channel set A. We note that at least for this data set, the spectrum reconstruction is nearly insensitive to a small change in the center wavelengths and widths of the selected channels. This result can be explained because the modified channels still lie partly in the spectral region where the values of the first eigenvector are large. Should we have chosen a channel completely outside of this spectral region, the standard deviation would have been dramatically increased as is shown in Figure 14 in which only the position of channel 3 was moved from 8.5-8.9 μm to 9.2-9.6 μm.

4.2. Error Analysis

Considering that reflectance measurements are made with random error σ_{m_i}, the resulting error on the reconstructed spectrum, $\sigma_x(\lambda)$ can be derived by applying the error theory to (6). It is given by

$$\sigma_x(\lambda) = \sqrt{\sum_{i=1}^{M} \left(a_i^2(\lambda)\sigma_{m_i}^2\right)} \le \sqrt{\sum_{i=1}^{M} a_i^2(\lambda)}\ \sigma_m^{\max}, \qquad (10)$$

where $\sigma_m^{\max}$ is the maximum random error made on the measurements among M channels.

Expression (10) shows that the error on the reconstructed spectrum is amplified by an amplification factor $A(\lambda)$:

$$A(\lambda) = \sqrt{\sum_{i=1}^{M} a_i^2(\lambda)}\,. \qquad (11)$$

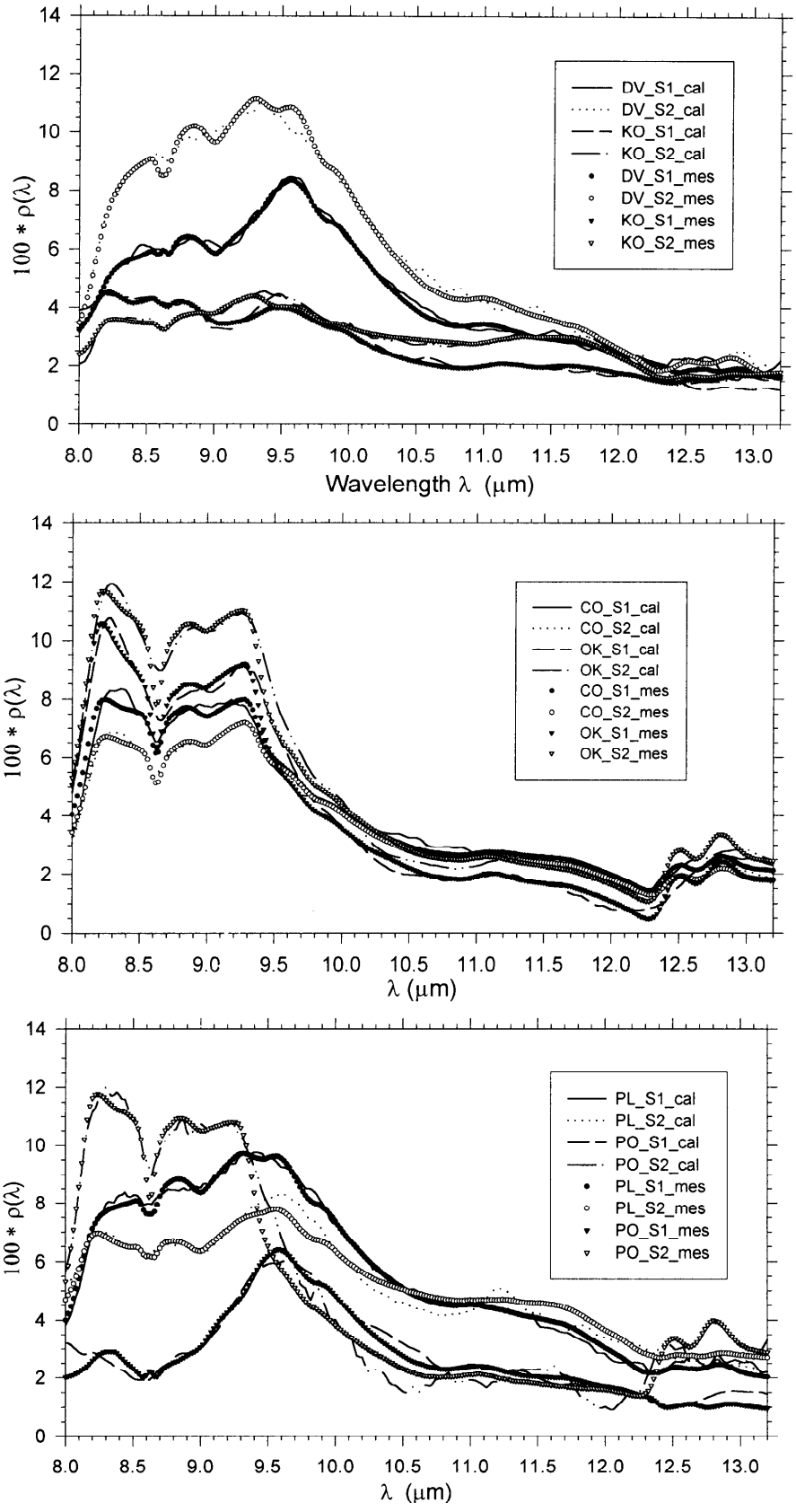

Figure 12. Same as Figure 10 but for a few soil samples in the UCSB data set. Here S1 and S2 represent sample 1 and sample 2, respectively. Additional abbreviations are as follows: DV, Death valley soil; KO, Koehn soil; CO, Concord soil; OK, Oklahoma soil; PL, Railroad valley playa soil; and PO, Railroad valley soil powder.

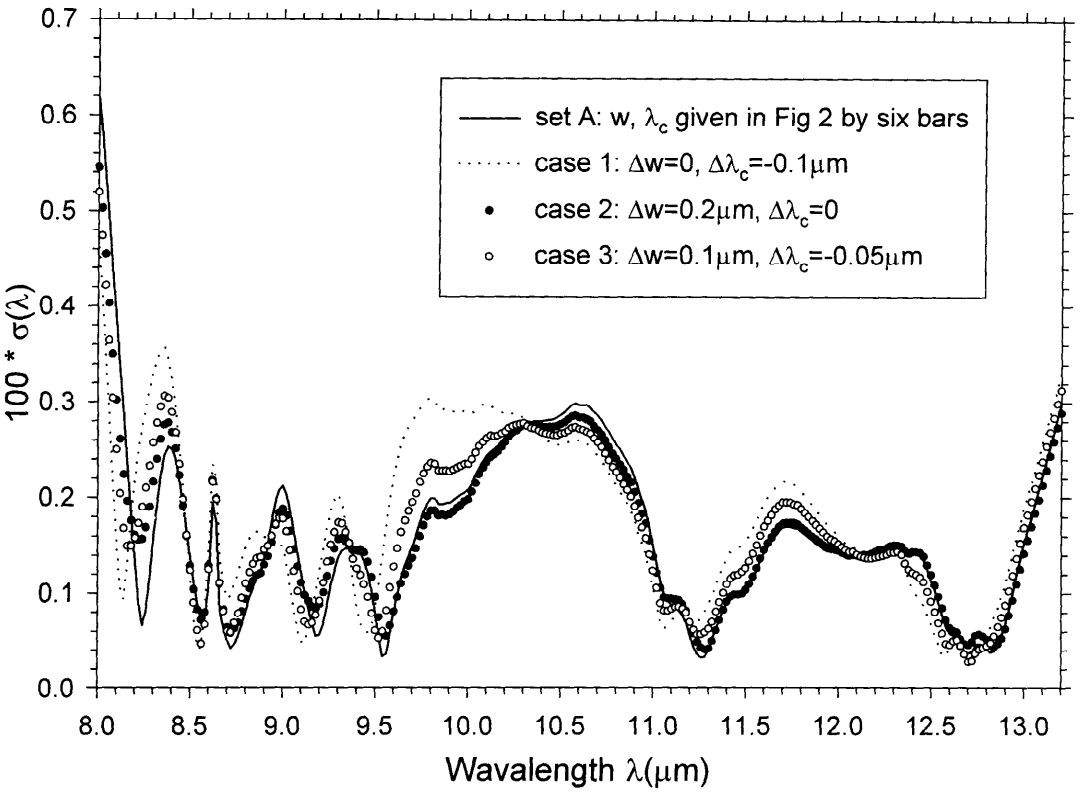

Figure 13. Standard deviation for each wavelength between the measured and reconstructed reflectance spectra using six channels of set A with different center wavelengths and/or different widths. $\Delta\lambda_c$ is the difference between the channel wavelength center in the study case and that indicated in Figure 2. Δw has the same meaning as $\Delta\lambda_c$ but for channel width.

Figure 15 displays the magnitudes of the amplification factor $A(\lambda)$ for both channel set A and set B. We note that the amplification factor in the reconstruction of the spectrum is smaller using channel set A than using channel set B. Should we have chosen the positions of channels 4 and 6 at their right positions (as channels in set A), the error on the reconstructed spectrum in the spectral regions 9.4-10.0 μm and 12.4-13.1 μm would have been reduced by about 50%. Furthermore, comparing the amplification factor of the channel set A with the amplification factors of the three cases used in the sensitivity analysis of section 4.1, Figure 16 illustrates that if the standard deviation is not sensitive to a small change of channel positions, the amplification factor is.

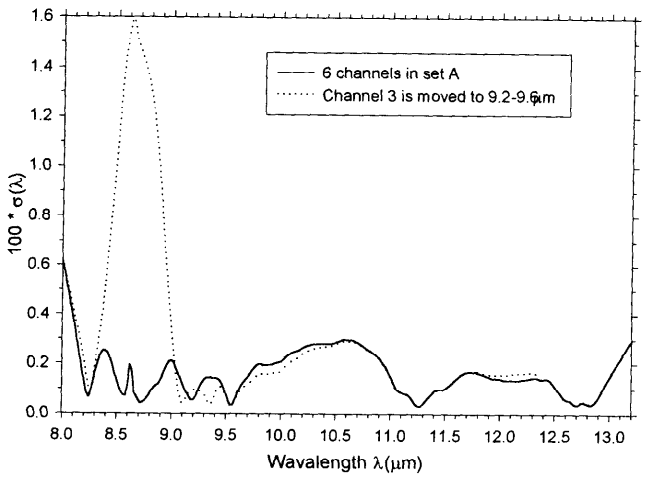

Figure 14. Standard deviation for each wavelength between the measured and reconstructed reflectance spectra with six channels: Channel set A and channel set A with the position of channel 3 moved to the spectral region 9.2-9.6 μm outside of the spectral region where the values of the first eigenvector are large (see Figure 2).

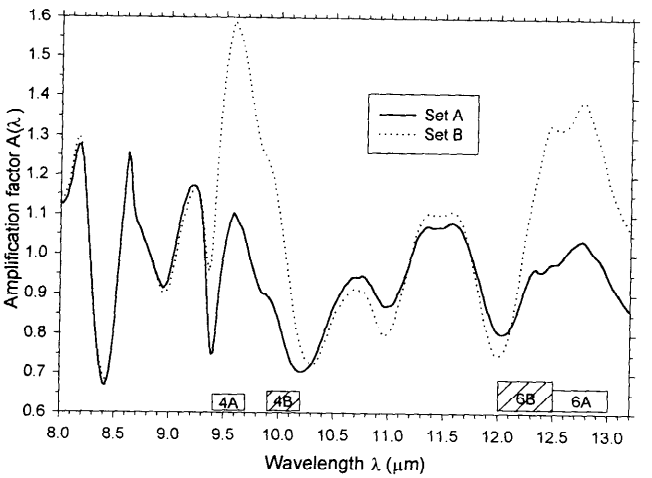

Figure 15. Amplification factors $A(\lambda)$ for both channel sets A and B in the propagation of the measurement errors.

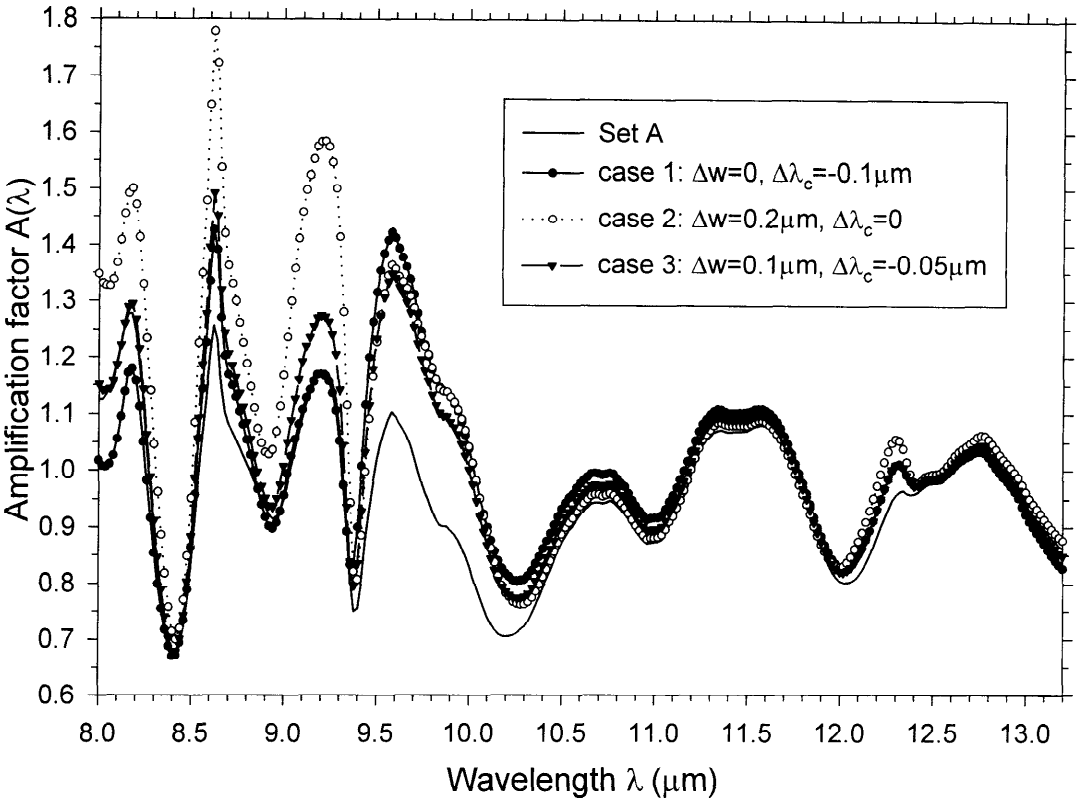

Figure 16. Same as Figure 15 but for the study cases used in Figure 13.

This brief analysis shows that the choice of the position and width of the selected channel has an important impact on the error generated in the reconstructed spectrum by the errors of measurements. It shows that for these cases the positions and widths given by the proposed scheme lead to the smallest error. Since this error is proportional to the amplification factor $A(\lambda)$ given by (11), an optimal choice of channels should minimize this factor. The particular example presented in this paper shows that the procedure proposed here leads to such a minimization of $A(\lambda)$. The generalization of this result to all situations is in progress.

5. Possible Applications

Considering, for instance, a measurement ε_k^{α} made in channel k which is different from the M selected channels, from (7) and (6), one obtains

$$\varepsilon_k^{\alpha} = c_{k0} + \sum_{i=1}^{M} \varepsilon_i^{\alpha} c_{ki} \,, \tag{12}$$

where c_{ki} is the integral of $f_k(\lambda) a_i(\lambda)$ over the spectral domain of channel k, that is,

$$c_{ki} = \frac{\int_{\lambda_{k\,\min}}^{\lambda_{k\,\max}} f_k(\lambda)\, a_i(\lambda)\, d\lambda}{\int_{\lambda_{k\,\min}}^{\lambda_{k\,\max}} f_k(\lambda)\, d\lambda} \,. \tag{13}$$

These expressions show that any channel emissivity out of these M independent channels can be expressed by the linear combination of the M channel emissivities whatever the sample is. This indicates that it may be possible to (1) use a simple radiometer with the M specific (independent) channels to compare the emissivities measured in any other channels, even if these differ in positions and widths and, (2) determine both surface temperature and channel emissivities from multispectral channel radiance if the channel number is greater than M (M independent channels). In fact, if a radiometer has N channels ($N \geq M$), there are N values of spectral radiance (measurements) and N+1 unknowns (N emissivities (one per channel) plus one surface temperature). Since the N emissivities are not independent and there are N-M linear relationships among the emissivitics as shown by (12), we have therefore in total $2N$-M equations for N+1 unknowns. Theoretically, if $N \geq (M+1)$, the system is overdetermined. This method may be applicable only if the surface spectral characteristics are retrieved by (12). Thus it is important to know what are the general characteristics of the observed surface with help of the visible and near-infrared data.

6. Conclusion

A procedure developed for channel selection in the visible and near-infrared region has been applied to thermal infrared region in 8-13 μm for soil spectra reconstruction. The results of this study show that the reflectance (or emissivity) measurements in the six appropriate channels lead to accurate reconstruction of soil spectra in 8-13 μm for most species. They also show that the process proposed by Price for the channel selection minimizes, at least for the cases studied, the measurement error propagation to the whole reconstructed spectrum. Furthermore, the sensitivity and error analyses

show that the reconstruction of the spectrum is nearly insensitive to a small change in the central wavelengths and widths of the selected channels if there are no measurement errors introduced. The numerical analysis of the data sets used in this paper show that if the measurement errors are taken into account, the resulting errors on this reconstructed spectrum are increased by such a change. In other words, if each measurement is made with a random error, the resulting errors on the reconstructed spectrum are the smallest when the measurements are made in the spectral channels selected by the proposed process.

The results of this study indicate that it may be possible to use instruments with the six specific channels to reconstruct the full spectrum of the soils, at least for the data sets used in this paper, and therefore to compare the results with other measurements even if they are made in channels with different positions and widths. In that case, any channel emissivity of soils out of those six channels can be expressed by the linear combination of the six channel emissivities; it appears to be possible to determine both surface temperature and channel emissivities of these soils from multispectral channel radiance if the channel number is greater than six.

As emphasized in the introduction, the six channels selected for these soils may not be applicable without extension to the reconstruction of the spectrum for other materials such as rocks and minerals. Furthermore, since this paper uses laboratory data as an illustration, the practical results obtained cannot be extended to remote sensing data without addressing, for instance, the problems related to atmospheric corrections and temperature/emissivity separation as well as the instrument noise. Therefore the selection of channels proposed in this paper to reconstruct soil spectra from in situ measurements may not be optimal for more general situations. Nevertheless, the procedure proposed can be extended to remote sensing data of other materials, but appreciable future work has still to be done in order to address the impact of atmospheric effects, temperature/emissivity separation, noise of measurement as well as more complex spectra.

It should be also kept in mind that the soil spectra used here are just laboratory spectra and represent only a fraction of the types of surfaces present in the real world. This study using laboratory spectra constitutes only an ideal case, and work is in progress to apply the technique used here to select the optimum channels for determining both surface temperature and emissivity from real or simulated remote sensing data.

Acknowledgments. We express our gratitude to J. Salisbury at JHU for providing us with the spectral data in digital form. Z.-L. Li wishes to thank M.P. Stoll at LSIIT and the CNRS for allowing him to leave Strasbourg in 1998 and Z. Wan at UCSB for providing him with the financial support during his stay at UCSB. Part of this work has been carried out under the European Space Agency contract 12076/96/NL/CN, and Z. Wan is supported by the NASA contract NAS5-31370. We thank two anonymous reviewers for their helpful and stimulating comments that greatly improved the quality of the manuscript.

References

Becker, F., The impact of spectral emissivity on the measurements of land surface temperature from a satellite, *Int. J. Remote Sens., 8*(10), 1509-1522, 1987.

Kahle, A.B., F.D. Palluconi, S. Hook, V. Realmuto, and G. Bothwell, The advanced spaceborne thermal emission and reflectance radiometer (ASTER), *Int. J. Imaging Syst. Tech., 3*, 144-156, 1991.

Price, J.C., Information content of IRIS spectra, *J. Geophys. Res., 80*, 1930-1936, 1975.

Price, J.C., On the information content of soil reflectance spectra, *Remote Sens. Environ., 33*, 113-121, 1990.

Price, J.C., Band selection procedure for multispectral scanners, *Appl. Opt., 33*, 3281-3288, 1994.

Price, J.C., Spectral band selection for visible near-infrared remote sensing: Spectral-spatial resolution tradeoffs, *IEEE Trans. Geosci. Remote Sens., 35*(5), 1277-1285, 1997.

Salisbury, J.W., and D.M. D'Aria, Emissivity of terrestrial materials in the 8-14 μm atmospheric window, *Remote Sens. Environ., 42*, 83-106, 1992.

Salisbury, J.W., and D.M. D'Aria, Emissivity of terrestrial materials in the 3-5 μm atmospheric window, *Remote Sens. Environ., 47*, 345-361, 1994.

Salisbury, J.W., D.M. D'Aria, and A. Wald, Measurement of thermal infrared spectral reflectance of frost, snow, and ice, *J. Geophys. Res., 99*, 24,235-24,240, 1994.

Snyder, W.C., Z. Wan, Y. Zhang, and Y. Feng, Thermal infrared (3-14 μm) bidirectional reflectance measurements of sands and soils, *Remote Sens. Environ., 60*, 101-109, 1997.

F. Becker, Z.-L. Li, and M.P. Stoll, Laboratoire des Sciences de l'Image, de l'Informatique et de la Télédétection, 5 Bd. Sebastien Brant, 67400 Illkirch, France. (becker@isu.isunet.edu; li@sahel.u-strasbg.fr; Marc-Philippe.Stoll@mail-grtr.u-strasbg.fr)

Z. Wan and Y. Zhang, Institute for Computational Earth System Science, University of California, Santa Barbara, CA93106-3060. (wan@icess.ucsb.edu; zhang@icess.ucsb.edu)

(Received January 12, 1999; revised May 17, 1999;
accepted June 22, 1999)